SCIENCE CHINA
Information Sciences

• RESEARCH PAPER •

June 2015, Vol. 58 062306:1–062306:10
doi: 10.1007/s11432-014-5266-6

System design and first airborne experiment of sparse microwave imaging radar: initial results

ZHANG BingChen[1,2], ZHANG Zhe[1,2,3*], JIANG ChengLong[1,2,3], ZHAO Yao[1,2], HONG Wen[1,2] & WU YiRong[1,2]

[1]*Science and Technology on Microwave Imaging Laboratory, Chinese Academy of Sciences, Beijing* 100190*, China;*
[2]*Institute of Electronics, Chinese Academy of Sciences, Beijing* 100190*, China;*
[3]*University of Chinese Academy of Sciences, Beijing* 100190*, China*

Received May 7, 2014; accepted November 4, 2014; published online April 10, 2015

Abstract In this paper, we mainly study the system design of sparse microwave imaging radar and report some of the preliminary results of airborne experiments performed with it. Sparse microwave imaging radar is a novel concept which introduces the sparse signal processing theory to microwave imaging replacing the conventional matched filtering processing method. With the exploitation of the sparse microwave imaging, the radar system could achieve better performance. As a newly developed concept, the two main types of applications of sparse microwave imaging are found in adopting the sparse signal processing theory to current radar systems, and in designing an optimized sparse microwave imaging system. Here we are trying the latter that mainly aims at lower PRF and wider swath. We first introduce the theories of sparse microwave imaging radar and its imaging algorithm. Then we discuss the system designing principles, including the sampling scheme, signal bandwidth, SNR and multi-channel mode. Based on the relationships of these parameters, we provide a design example of radar parameters. In the end, we exploit an airborne experiment using our designed radar system with jittered azimuth sampling strategy. Some preliminary analysis from the experiment result is also provided.

Keywords sparse microwave imaging, synthetic aperture radar (SAR), compressive sensing, displaced phase center antenna (DPCA), system design, airborne experiment

Citation Zhang B C, Zhang Z, Jiang C L, et al. System design and first airborne experiment of sparse microwave imaging radar: initial results. Sci China Inf Sci, 2015, 58: 062306(10), doi: 10.1007/s11432-014-5266-6

1 Introduction

Synthetic aperture radar (SAR) usually cited as "microwave imaging", is one of the main technologies of modern remote sensing. Modern SAR systems commonly aim at two key features of system performance: wide mapping swath and high imaging resolution. According to the SAR theory, wider swath means a larger observing area with more imaging data, higher resolution that requires a wider signal bandwidth, resulting in a higher sampling rate and a higher amount of data because of the Nyquist theorem. So, as the swath and resolution increase, the SAR system complexity and data amount also increase remarkably, which brings difficulties to the hardware implementation, and limits the future evolution of SAR systems. This is a bottleneck. Furthermore, high resolution and wide swath themselves are a pair of contradictories.

* Corresponding author (email: pzhgrsrs@gmail.com)

Higher resolution requires higher pulse repetition frequency (PRF), but high PRF limits the increment of swath.

Some features of radar imaging, e.g. the sparsity of target scene, could be used to deal with these problems. Since in many cases, the SAR target scene is sparse, i.e. there only exist a few non-zero targets in the whole scene, we can introduce the sparse signal processing theory to the microwave imaging. Sparse signal processing was developed by mathematicians by the end of 20th century [1]. A main component of sparse signal processing was named as compressive sensing (CS) [2–5]. According to CS, a sparse signal can be perfectly reconstructed with much fewer samples than that required by Nyquist theorem.

Many works have been done to introduce the afore-mentioned sparse signal processing technology to conventional microwave imaging radar to develop the concept of sparse microwave imaging [6–8], aiming at achieving benefits in reducing the system complexity and improving the system performance. There exist two types of applications of sparse microwave imaging. First, adopting the signal processing method of sparse microwave imaging to current radar systems. It means, we use some achievements of sparse microwave imaging theory to improve the performance of existing SAR systems [9]. Second, designing a fresh-new radar system under the guidance of sparse microwave imaging theory. In this paper we focus on the latter application. We call it an "optimized" sparse microwave imaging radar.

Compared with the conventional SAR, the sparse microwave imaging system might have greater potential to reduce the system data amount and complexity, and improve system performance in many aspects, for example, lower requirements in azimuth and range sample rates, higher distinguishing ability, lower ambiguity, lower system complexity and less data amount [7]. Not all these advantages can be reflected in a single design. In this paper, we mainly focus on the reduction of PRF and improvement of swath during the system design. The sparse sampling could be applied in the azimuth direction, i.e. the constraint of PRF could be relaxed. As a result, the selection range of swath will be larger than that in conventional SAR. In displaced phase center antenna (DPCA) [10] case, the constraint of PRF will be even looser such that wider swath can be achieved with utilizing the sparse microwave imaging.

In September 2013, we carried the first proof-of-principle airborne experiment in Tianjin, China using our designed sparse microwave imaging radar system. This is an optimized designed sparse microwave imaging radar system with specific design azimuth sampling scheme. The experiment data is still under review. Some initial results of experiment will be introduced in this paper.

This paper is organized as follows. In Section 2, the sparse microwave imaging theory and imaging algorithm are introduced. The principles of system design are discussed in Section 3. An example of system parameter design is given in Section 4. The airborne experiment is provided in Section 5 as the verification of designing principles. Conclusion is in Section 6.

2 Model and imaging algorithm

This section briefly recalls the sparse microwave imaging theory. The theoretical description of the sparse observation model is summarized and the reconstruction algorithm which directly processes the raw data is discussed too. The sparse microwave imaging method is feasible in real data experiments and gives an improvement of imagery quality in contrast to the conventional algorithm. Most importantly, by using sparse microwave imaging concept it is possible to propose a novel imaging system that should pave the way for many new applications that are highly desirable.

2.1 The system model

The sparse microwave imaging radar system model is given as [7]

$$\boldsymbol{y} = \boldsymbol{\Phi} x + \boldsymbol{n} = \boldsymbol{\Theta H \Psi} \alpha + \boldsymbol{n}, \tag{1}$$

where $\boldsymbol{y}$ is the measured echo data, $\boldsymbol{x}$ is the back-scattering coefficients of the scene, $\boldsymbol{n}$ is the additive noise, and $\boldsymbol{\Phi}$ is the measurement matrix of radar system, it is defined as $\boldsymbol{\Phi} = \boldsymbol{\Theta H}$ with $\boldsymbol{\Theta}$ being the matrix for the sparse/compressed sampling strategy of the radar echoes and $\boldsymbol{H}$ being the observation matrix of

radar system. The terminology "observation matrix" here is different from "measurement matrix", for the "measurement matrix" in equation (1) in fact includes two components: observation and sampling. Observation matrix $\boldsymbol{H}$ only refers to the former one, and it is determined by the radar hardware. The vector $\boldsymbol{x}$ can be decomposed into $\boldsymbol{x} = \boldsymbol{\Psi}\alpha$ with $\boldsymbol{\Psi}$ being a dictionary and α being corresponding sparse coefficient vector. The detailed expression of these matrices and vectors can be found in [7,11].

According to the afore-mentioned sparse signal processing theory, x can be reconstructed by

$$\hat{\boldsymbol{x}} = \boldsymbol{\Psi} \cdot \{\arg\min_{\boldsymbol{\alpha}} \|\boldsymbol{\alpha}\|_1, \quad \text{s.t. } \|\boldsymbol{y} - \boldsymbol{\Theta}\boldsymbol{H}\boldsymbol{\Psi}\boldsymbol{\alpha}\|_2 < \epsilon\}, \tag{2}$$

where $\epsilon = \|\boldsymbol{n}\|_2$. When the observed scene is presumed as sparse, then the $\boldsymbol{\Psi}$ is chosen as identity matrix, which means it contains very few dominate scattering targets in the whole scene. In this situation the reconstruction of the scene is given by

$$\hat{\boldsymbol{x}} = \arg\min_{\boldsymbol{x}} \|\boldsymbol{x}\|_1, \quad \text{s.t. } \|\boldsymbol{y} - \boldsymbol{\Phi}\boldsymbol{x}\|_2 < \epsilon. \tag{3}$$

2.2 The reconstruction algorithm

Recently, many researchers have tried the combination of sparse signal processing method and the conventional radar imaging framework. Moreover, such kind of methods can be ameliorated by decoupling the azimuth and range of the raw data to uplift the computation efficiency [12]. The concept of decoupling azimuth and range lies in the formation of SAR signal from the reflective image of the observation area. Intuitively, the measurement matrix can be analyzed as a azimuth convolution matrix $\boldsymbol{H}_a$ imposed on the reflective image to obtain Doppler history, a range-azimuth migration operator $\mathcal{M}(\cdot)$ to generate two-dimensional impulse response, and a range convolution matrix $\boldsymbol{H}_r$ to complete the 2D echo signal $\boldsymbol{Y}$:

$$\boldsymbol{Y} \approx \boldsymbol{\Theta}\left(\mathcal{M}\left(\boldsymbol{H}_a \cdot \boldsymbol{X}\right)\boldsymbol{H}_r\right), \tag{4}$$

where $\boldsymbol{X}$ is the 2D SAR image obtained by reshaping the column vector $\mathbf{x}$ to 2-D grid range-wisely. The state-of-art SAR imaging algorithms are suitable for implementation of the approximate procedure and similar accelerated algorithm has been applied to real data with uniform sampling schemes.

The sparse microwave imaging algorithms are also applicable to multi-channel SAR systems [10]. The conventional multi-channel imaging algorithm is based on frequency reconstruction [13]. It is able to recover the true spectrum from the nonuniform samples, however the performance is sensitive to the selection of PRF. A frequency domain method based on sparse regularization technique shows the robustness of non-uniform sampling scheme towards azimuth direction [14]. The decoupled model for channel i can be formulated as follows,

$$\boldsymbol{Y}_i = \mathcal{G}_i\{\boldsymbol{X}\} + \boldsymbol{N}_i, \tag{5}$$

where $\boldsymbol{Y}_i$ represents the echo of channel i, $\boldsymbol{X}$ is the 2D full-resolution SAR image, and $\mathcal{G}_i\{\cdot\}$ stands for the operator that exploits $\boldsymbol{X}$ to generate the echo signal of channel i,

$$\mathcal{G}_i\{\boldsymbol{X}\} = \boldsymbol{F}'_a(\boldsymbol{S} \odot \mathcal{T}\{\boldsymbol{P}_i \odot (\boldsymbol{F}_a\boldsymbol{X})\boldsymbol{F}_r\}\boldsymbol{F}'_r \odot \boldsymbol{Q}), \tag{6}$$

where $\odot$ stands for Hadamard multiplication, $\boldsymbol{F}$ and $\boldsymbol{F}'$ are the discrete fourier transform matrix and its inverse matrix. The subscripts a and r refer to the azimuth and range directions respectively. $\boldsymbol{P}_i(m,n) = \exp\left\{\mathrm{j}\pi f_a^2(m)/k_a(n)\right\}\cdot\exp\{-\mathrm{j}\pi\Delta x_i(n)f_a(m)/v\}$ denotes the azimuth convolution matrix which multiplies the phase that requires channel i and v for the platform velocity, $f_a(m)$ is the azimuth frequency in the mth row, $k_a(n)$ is the azimuth modulation rate in the nth column and $\Delta x_i(n)$ is the distance between the ith receiving antenna to the transmitting antenna. $\mathcal{T}\{\cdot\}$ folds the azimuth spectrum due to the sub-sampling. $\boldsymbol{Q}$ and $\boldsymbol{S}$ are carried out using the standard phase functions $\boldsymbol{\Phi}_1$ and $\boldsymbol{\Phi}_2$ of chirp scaling algorithm [15]. By combining all the channels, the reconstruction written as,

$$\hat{\boldsymbol{X}} = \arg\min_{\hat{\boldsymbol{X}}} \sum_i \| \boldsymbol{Y}_i - \mathcal{G}_i\{\hat{\boldsymbol{X}}\} \|_2^2 + \mu \| \hat{\boldsymbol{X}} \|_1, \tag{7}$$

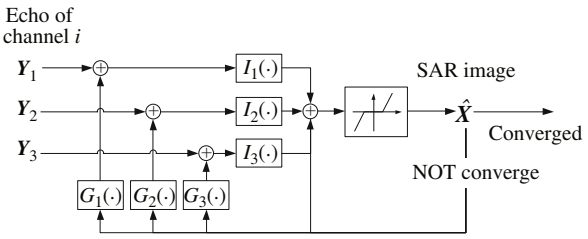

Figure 1 The iterative spectrum reconstruction for multichannel subsampling in case of three channels.

where μ is the regularization parameter.

This is an ℓ_1 regularization problem [16]. For instance, we use a three-channel model. The diagram of the iterative spectrum reconstruction algorithm for solving (7) is shown in Figure 1 [14]. The SAR image contains full bandwidth doppler spectrum. The estimated signal for channel i, $i = 1, 2, 3$ is obtained by respectively applying $\mathcal{G}_i\{\cdot\}$ on $\hat{\boldsymbol{X}}$ and the bandwidth to one third of the full one. The residual echo signal $\boldsymbol{Y}_i - \mathcal{G}_i\{\hat{\boldsymbol{X}}\}$ then passes through the imaging operator $\mathcal{I}_i\{\cdot\}$ and forms a newly designed SAR image. As can be inferred above, $\mathcal{G}_i\{\cdot\}$ is linear and $\mathcal{I}_i\{\cdot\}$ is the conjugate transpose of $\mathcal{G}_i\{\cdot\}$. In the next step, the thresholding function is applied to regularize the current estimation of $\hat{\boldsymbol{X}}$.

2.3 Evaluation [7, 17]

As the sparse microwave imaging is based on a nonlinear framework, the classic evaluation tools of imaging radar are no longer applicable here. New evaluation tools are required. To evaluate radar system performance, we suggest the use of three-dimensional phase transit diagrams [17].

3 Sparse microwave imaging system design principles

In this section, we will discuss the principles for designing sparse microwave imaging system. As discussed before, not all advantages of sparse microwave imaging can be included in a single design. In this paper, we mainly focus on one improvisation brought about by sparse microwave imaging which is the requirement of lower PRF for achieving wider swath.

Firstly, we will introduce the sampling schemes of sparse microwave imaging especially in the azimuth direction. As per earlier report, a random under-sampling provides the best reconstruction performance [18]. The random sampling has the lowest sampling rate requirement and the best reconstruction probability. But a completely random sampling has an obvious disadvantage. Though the average sampling rate under this scheme could be quite low, the minimal interval between two samples might be very short i.e. the maximal instantaneous sampling rate might be very high. Hence, the observation swath is still limited. As a solution, a random under-sampling with guaranteed minimal pulse repetition time (PRT) is exploited to reduce PRF and increase the swath. Examples of such sampling schemes include jittered sampling [7,19,20] and Poisson disk sampling [21], here we use the jittered sampling.

Secondly, we suggest that the imaging swath could be even increased with applying the dual/multi-channel technologies. The selecting range of PRF is even looser under the multi-channel constraints.

Finally, the considerations of related radar parameters such as bandwidth, SNR and beam scanning are discussed.

3.1 Sampling scheme

Different sampling schemes lead to different imaging performance. Advantages and disadvantages of different sampling schemes have been discussed in detail in [7]. In this paper, we mainly consider the jittered under-sampling strategy as the sampling scheme for sparse microwave imaging. Implementation of such scheme is relatively simple and requires a minor change to the PRF scheduling of the radar as it is aimed at modifying the PRF of the radar. The under-sampling scheme is based on a regular under-sampling which is perturbed slightly by a random distributed jittering. It is shown in Figure 2. As the

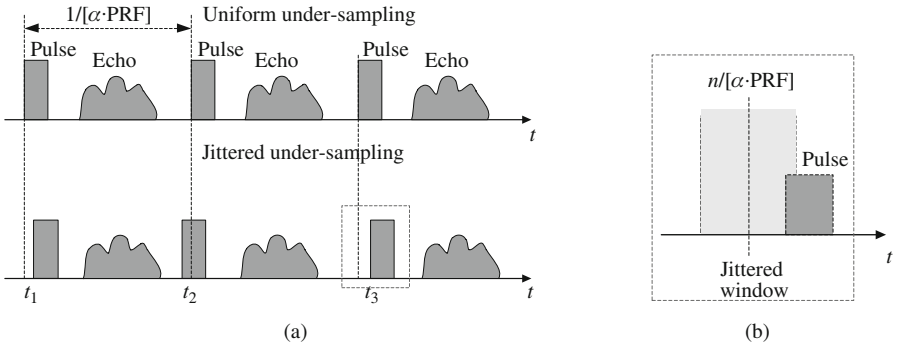

Figure 2 Jittered under-sampling scheme. (a) Compared with uniform under-sampling scheme, the sampling time of jittered under-sampling scheme is perturbed by additional factor; (b) the zoomed out of the red dash rectangle.

radar moves along its path, the nth pulse is transmitted at t_n, which is expressed as:

$$t_n = n/\left[\alpha \cdot \mathrm{PRF}\right] + \epsilon_n, \tag{8}$$

where PRF is the conventional pulse repetition frequency, $\alpha \in (0, 1]$ is the under-sampling factor, ϵ_n is the perturbing factor. Assume that ϵ_n is a uniform random variable which distributes in $[-t_p/2, t_p/2]$. Then the sampling interval $\Delta t_n = t_n - t_{n-1}$ is between $[\alpha \cdot \mathrm{PRF} - t_p, \alpha \cdot \mathrm{PRF} + t_p]$.

The jittered under-sampling scheme serves two major purposes. Firstly, by under-sampling in the azimuth direction and by reconstructing employing sparse microwave imaging method, it enlarges the swath. Secondly, the random changes imposed on the regular PRT can break up the periodicity of the aliasing artifacts and preserve the high frequency energy [20].

3.2 PRF selection

The sparse microwave imaging also has the potential to ease constraints on the selection of PRF for multi-channel imaging radar system, or the displaced phase center antenna (DPCA) mode. In a single-platform multi-channel system, the channel distance and the platform velocity are fixed and a specific PRF will be required [22]

$$\mathrm{PRF}_{\mathrm{opt}} = \frac{2 \cdot v}{I \cdot d_r}, \tag{9}$$

where v is the platform velocity, $I \geqslant 2$ is the number of channel, d_r is the subaperture distance. Under this PRF, a spectrum reconstruction method was proposed which could significantly suppress the ambiguous energy [13]. However, such a reconstruction is sensitive to PRF and not adaptive to under-sampling. It means that, such optimized PRF must be precisely followed as shown in Figure 3(a). If not so, recovery error would occur leading to failure in imaging. Unfortunately, such a rigid selection of the PRF may be in conflict with the timing diagram for some incident angles, i.e. sometimes the optimized PRF would cause quite a narrow swath.

The sparse microwave imaging method can be used to overcome this conflict. By utilizing sparse reconstruction algorithms, We can loose the constraint of PRF and exploit the random sampling scheme along azimuth direction. With regard to system design, it would be advantageous to take more PRF selections (compared to only one optimized candidate PRF) to avoid conflict in timing diagram and obtain a wider swath.

3.3 Bandwidth, SNR, and beam scanning, etc.

Here we will discuss the considerations of other related radar parameters. Starting with the signal bandwidth. Both theoretical research and experiments show that the bandwidth requirement of sparse microwave imaging system is at the same level as in the conventional imaging radar system [7]. It means that the signal bandwidth is selected under the same constraint as in the conventional SAR according

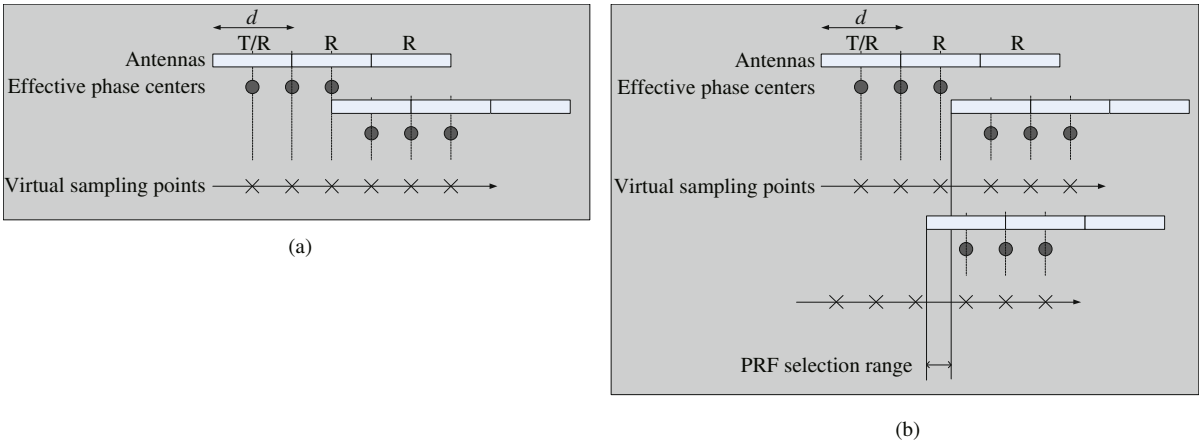

Figure 3 The sparse microwave imaging looses the constraint of PRF for dual/multichannel SAR. (a) In conventional DPCA the PRF is restricted; (b) the sparse microwave imaging looses the constraint of PRF.

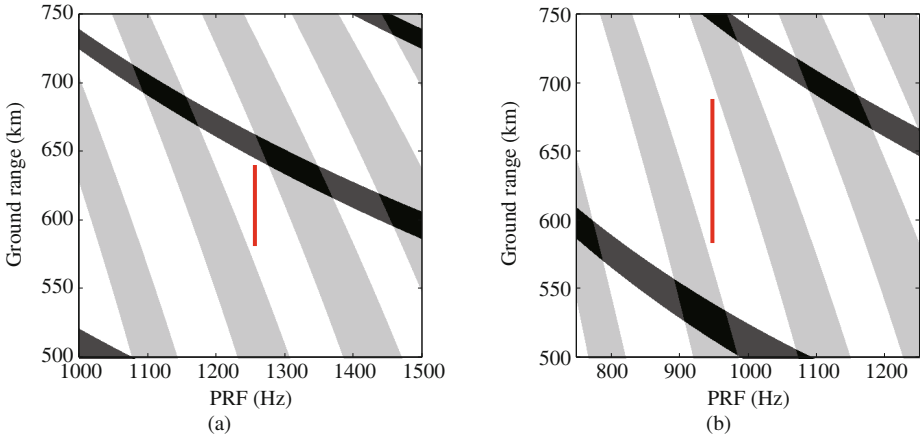

Figure 4 Illustration of obtaining wider swath by the application of sparse sampling. (a) The 2nd beam of RadarSat Fine mode, PRF = 1257 Hz, which covers the incident angle between 39.3° and 42.1°, about 50 km ground range swath; (b) our design using sparse microwave imaging scheme with PRF = 947 Hz, the swath is approximately 100 km.

to the discrimination of the required system. While, if the scene is sparse, the distinguishing ability of imaging system could be enhanced. Secondly, the SNR and transmitting power. In the sparse microwave imaging theory, a minimal system SNR is required. If the SNR is too low, the sparse reconstruction might fail. So the system SNR must be acceptable within the limits. Simulations and experiments show that the SNR that is at the same level of conventional SAR is enough for sparse reconstruction [7]. This requirement could be satisfied by enhancing the transmitting power, expanding the pulse duration time and enlarging the antenna area. Thirdly, the beam scanning technologies, for example the ScanSAR [23] and TOPSAR [24], could also be used to increase the system swath. In this case, the system designing principles are kept constant.

4 Design examples

This section gives an example of SAR system design to demonstrate the applicability and potentials of the sparse microwave imaging framework to obtain wider swath with higher geometric resolution. The selection of key parameters for imaging is mainly based on the fine mode of RadarSat system [25]. Afterwards, a performance analysis is carried out.

The example of the design is provided to prove that by sparse sampling in azimuth direction, we can obtain wider swath. The timing diagram is shown in Figure 4. The F2 beam of RadarSat fine mode in

Table 1 System design parameters for single channel

	F2 beam of RadarSat fine mode	Our design
Incident angle (°)	39.3–42.1	39.1–44.9
PRF (Hz)	1257	947
Swath width (km)	50	100
Bandwidth (MHz)	26	26
Azimuth resolution (m)	9	9
Range resolution (m)	10	10
Pulse duration (μs)	42	55
Raw data rate (Mbps) (Estimated using 8bit quantization)	200	280
Average radiated power (W)	300	300
NEσ^0 (dBm^2/m^2)	−25	−25

Table 2 System design Parameters for dual channels

	Routine DPCA	DPCA + sparse
Incident angle (°)	35.1–37.1	35.0–40.5
PRF (Hz)	1491	1147
Swath width (km)	30	90
Bandwidth (MHz)	80	80
No. of sub-apertures	2	2
Azimuth resolution (m)	3	3
Range resolution (m)	3	3
Pulse duration (μs)	42	50
Raw data rate (Mbps) (Estimated using 8bit quantization)	800	1500
Average radiated power (W)	350	350
NEσ^0 (dBm^2/m^2)	−21	−21

the timing diagram is shown in Figure 4(a), which has 50 km swath width with the PRF of 1257 Hz. In our design, the azimuth sampling rate is reduced to 947 Hz, which is 76% of the classical one and is numerically justified for imaging the sparse scene. The PRF selection for sparse microwave imaging is shown in Figure 4(b). The incident angle varies from 39.1° to 44.9°, covering about 100 km swath coverage, which is twice compared to the fine mode beam. The parameters are listed in Table 1.

The performance analysis is also given in Table 1. In this design the range sampling rate is set to 1.2·Br, where Br denotes the bandwidth of the transmitted signal. The received echo is quantified with 8bit width in both I/Q channel. To keep the signal noise ratio (SNR) in the same level, we consider increasing the duration of the transmit pulse. Received noise coefficient is 3.5 dB. Received noise temperature is 795 K.

The dual channel mode can also exploit the sparse microwave imaging to loose the selection of PRF and achieve even higher swath. We simulate the DPCA system parameters by using the parameters of ultrafine mode of Radarsat-2 as the reference. The ultra-fine mode in the timing diagram has 30 km swath width with $\mathrm{PRF}_{\mathrm{opt}} = 1491$ Hz. In our design, the azimuth sampling rate is reduced to 1147 Hz, which is 77% of the conventional one. In Table 2, the DPCA together with sparse microwave imaging increases the swath to 3 times of the routine DPCA. The sparse microwave imaging can be applied to TOPS mode to obtain much more wider swath.

5 Results of first airborne experiment

The final purpose of studying these principles is to design a novel optimized sparse microwave imaging radar system. As an initial attempt, we will briefly introduce an airborne experiment that was con-

Table 3 Experiment setup and radar system parameters

Parameter	Value
Platform	Cessna "Citation"
Height	3900 m
Velocity	about 108 m/s
Bandwidth	500 MHz/80 MHz
Center frequency	5.6 GHz
Antenna azimuth length	0.9 m
Pulse duration	38 μs
PRF	Average 768 Hz

(a) (b) (c)

Figure 5 The imaging results of different azimuth sampling strategies. (a) The full-sampled target scene; (b) 60% uniform under-sampling; (c) 60% jittered under-sampling.

ducted in September 2013, Tianjin, China. In this experiment, we mainly test the jittered azimuth under-sampling. Other consideration e.g. the multi-channel will be verified in future experiments. We implemented the jittered azimuth sampling hardware.

5.1 Experiment setup

The system parameters are given in Table 3. We selected several locations in this experiment. All of them are sparse scenes including salt pans and harbors located by the seashore of Tianjin, China.

5.2 Initial result and analysis of jittered sampling

The experiment is still in pipeline. And the major results will be discussed in detail in our later publications. As one of the results of some initial analysis, we would like to demonstrate the effectiveness of jittered azimuth sampling here.

We select a sparse scene of salt pans as the target scene. The full-sampled image is shown in Figure 5. The estimated sparsity is about 4.5%, where the sparsity denotes the percentage of pixels that brighter than average. We achieve this same scene with two different azimuth sampling strategies: uniform 60% under-sampling and jittered 60% under-sampling (The percentage is compared with the Nyquist rate). The imaging results of two sampling schemes are given in Figure 6. From the figures it is quite clear that the result of uniform sampling fails to image in Figure 6(a), while the result of jittered sampling performs well in Figure 6(b).

We also used the phase transit diagram to evaluate the experimental result. Along with the experimental parameters, phase transit diagrams of both uniform and jittered sampling schemes are given in Figure 6. The phase transit diagram is calculated with SNR = 30 dB. The red area means the "fail" area, and the blue area denotes the "success" area. We can find that under the experimental condition, the uniform sampling drops into the "fail" area as shown in Figure 6(a), while the jittered sampling lies in the "success" area in Figure 6(b). This fits our experimental result precisely.

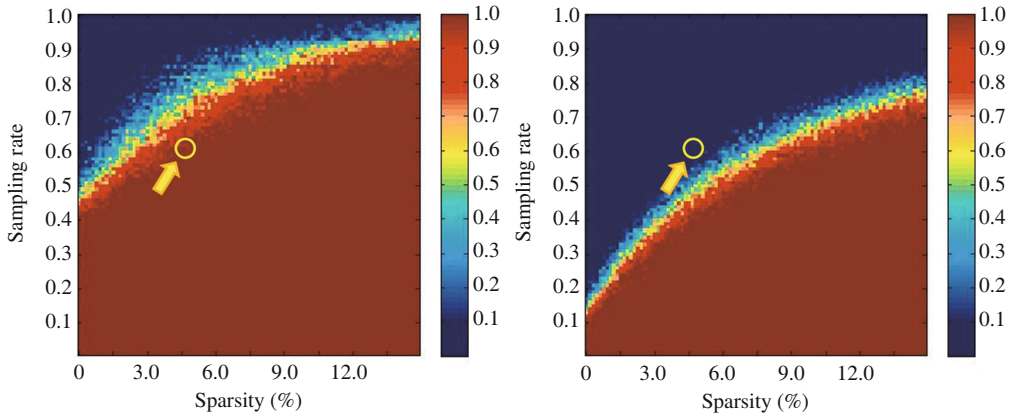

Figure 6 The phase transit diagram of different azimuth sampling strategies. Yellow circle is the point that represents the experiment parameters. (a) Uniform under-sampling; (b) jittered under-sampling.

6 Conclusion

In this paper we discussed the system design principles of sparse microwave imaging radars. The design principles include the system sampling, multi-channel mode and radar parameter selection. According to these principles, we suggest the design example, and verify the principles via experiments. The sparse microwave imaging system has many advantages. The reduction of PRF leading to increase of swath is only one aspect of it. The other potential advantages of sparse microwave imaging such as the increase of distinguishing ability and lower system complexity are not considered in the design example of this paper. Further work on both design principles and experiments are in progress.

Acknowledgements

This work was supported by National Basic Research Program of China (973 Program) (Grant No. 2010CB731905). We also want to express special thanks to the System Group of the Science and Technology on Microwave Imaging Laboratory (MITL) for their effort in experiment data acquisition.

References

1 Baraniuk R G, Candès E, Elad M, et al. Applications of sparse representation and compressive sensing. Proc IEEE, 2010, 98: 906–909
2 Donoho D L. Compressed sensing. IEEE Trans Inf Theory, 2006, 52: 1289–1306
3 Candès E J, Tao T. Near-optimal signal recovery from random projections: universal encoding strategies? IEEE Trans Inf Theory, 2006, 52: 5406–5425
4 Candès E J, Romberg J K, Tao T. Stable signal recovery from incomplete and inaccurate measurements. Commun Pure Appl Math, 2006, 59: 1207–1223
5 Hu L, Zhou J X, Shi Z G, et al. Compressed sensing of superimposed chirps with adaptive dictionary refinement. Sci China Inf Sci, 2013, 56: 122302
6 Rao W, Li G, Wang X Q, el al. Comparison of parametric sparse recovery methods for ISAR image formation. Sci China Inf Sci. 2014, 57: 022315
7 Zhang B C, Hong W, Wu Y. Sparse microwave imaging: principles and applications. Sci China Inf Sci, 2012, 55: 1722–1755
8 Ender J H G. On compressive sensing applied to radar. Signal Process, 2010, 90: 1402–1414
9 Jiang C L, Zhang B C, Zhang Z, et al. Experimental results and analysis of sparse microwave imaging from spaceborne radar raw data. Sci China Inf Sci, 2012, 55: 1801–1815
10 Currie A, Brown M A. Wide-swath SAR. IEE Proc Radar signal process, 1992, 139: 122–135
11 Zhang Z, Zhang B C, Jiang C L, et al. Influence factors of sparse microwave imaging radar system performance: approaches to waveform design and platform motion analysis. Sci China Inf Sci. 2012, 55: 2301–2317
12 Fang J, Xu Z, Zhang B, et al. Fast compressed sensing SAR imaging based on approximated observation. IEEE J Sel Top Appl Earth Obs Rem Sens, 2014, 7: 352–363

13 Krieger G, Gebert N, Moreira A. Unambiguous SAR signal reconstruction from nonuniform displaced phase center sampling. IEEE Geosci Rem Sens Lett, 2004, 1: 260–264
14 Fang J, Zeng J S, Xu Z B, et al. Efficient DPCA SAR imaging with fast iterative spectrum reconstruction method. Sci China Inf Sci, 2012, 55: 1838–1851
15 Raney R K, Runge H, Bamler R, et al. Precision SAR processing using chirp scaling. IEEE Trans Geosci Rem Sens, 1994, 32: 786–799
16 Daubechies I, Defrise M, De Mol C. An iterative thresholding algorithm for linear inverse problems with a sparsity constraint. Commun Pure Appl Math, 2004, 57: 1413–1457
17 Tian Y, Jiang C L, Lin Y G, et al. An evaluation method for sparse microwave imaging radar system using phase diagrams. In: Proceedings of CIE Radar Conference, Chengdu, 2011
18 Candès E, Romberg J. Sparsity and incoherence in compressive sampling. Inverse Probl, 2007, 23: 969–985
19 Patel V M, Easley G R, Healy D, et al. Compressed synthetic aperture radar. IEEE J Sel Top Signal Process, 2010, 4: 244–254
20 Balakrishnan A. On the problem of time jitter in sampling. IRE Trans Inf Theory, 1962, 8: 226–236
21 Geng B, Zhang H J, Wang H, el al. Approximate Poisson disk sampling on mesh. Sci China Inf Sci. 2013, 56: 092117
22 Curlander J C, McDonough R N. Synthetic Aperture Radar: Systems and Signal Processing. New York: Wiley, 1991
23 Cumming I G, Wong F H. Digital Signal Processing of Synthetic Aperture Radar Data: Algorithms and Implementation. Artech House, 2004
24 De Zan F, Guarnieri A M. TOPSAR: terrain observation by progressive scans. IEEE Trans Geosci Rem Sens, 2006, 44: 2352–2360
25 Raney R K, Luscombe A P, Langham E, et al. Radarsat. Proc IEEE, 1991, 79: 839–849